



Effects of surface heating on stability and transition in a supersonic nozzle boundary layer  
by Torence Patrick Brogan

A thesis submitted in partial fulfillment of the requirements for the degree of Doctor of Philosophy in  
Engineering (Applied Mechanics)  
Montana State University  
© Copyright by Torence Patrick Brogan (1999)

**Abstract:**

Acoustic fluctuations that originate from transitional and turbulent boundary layers in a supersonic wind tunnel limit the capabilities of ground test facilities for boundary layer transition research and testing. The present work explores boundary layer stability and transition with and without surface heating on one contoured wall of a low-disturbance Mach 3 two-dimensional wind tunnel at Montana State University.

The throat area of the lower contoured surface was heated to a steady state temperature of 13% and 22% over the stagnation temperature at unit Reynolds numbers of  $5.2 \times 10^6/m$  and  $6.2 \times 10^6/m$ , respectively. Boundary layer measurements with a small, fast-response, pitot probe were used to characterize fluctuation magnitude, frequency content, and the rate of amplification with and without surface heating. The effect of surface heating was to reduce the amplitude of a low frequency disturbance at all streamwise positions. Suppressing this low frequency activity caused turbulent bursting to be moved downstream, thereby increasing the extent of laminar flow to nearly the entire nozzle length. Predictions with linear stability theory showed that heat has a mild stabilizing effect on Gortler vortices, and first-mode Tollmien-Schlichting waves could be suppressed with a proper heating distribution by moving the neutral point downstream and reducing the subsequent amplification rates. However, the  $e^N$  method with linear stability theory completely failed to predict the observed transition in the nozzle boundary layer due to unsteady oscillations, even in the case without surface heating.

Calculations of the mean-flow also showed that natural cooling (heat followed by cooling) and roughness arguments do not appear to explain the observed stability events.

The experiment and theory show at least two different paths to turbulence suppression by heating the surface of a supersonic nozzle. (1) The experiment demonstrates that heat suppresses a bypass mechanism triggered by receptivity events near and possibly upstream of the nozzle throat. (2) The computations show that a proper heating distribution can also be used to suppress the growth of linear instabilities in the nozzle if bypass were not present.

EFFECTS OF SURFACE HEATING ON STABILITY AND TRANSITION  
IN A SUPERSONIC NOZZLE BOUNDARY LAYER

by

Torence Patrick Brogan

A thesis submitted in partial fulfillment of the  
requirements for the degree

of

Doctor of Philosophy

in

Engineering (Applied Mechanics)

MONTANA STATE UNIVERSITY  
Bozeman, Montana

January 1999

© COPYRIGHT

by

Torence Patrick Brogan

1999

All Rights Reserved

D378  
B7864

APPROVAL

of a thesis submitted by  
Torence Patrick Brogan

This thesis has been read by each member of the thesis committee and has been found to be satisfactory regarding content, English usage, format, citations, bibliographic style, and consistency, and is ready for submission to the College of Graduate Studies.

Dr. Anthony Demetriades      Anthony Demetriades      1/14/99  
Signature      Date

Approved for the Department of Mechanical and Industrial Engineering

Dr. Vic Cundy      Vic A. Cundy      1/14/99  
Signature      Date

Approved for the College of Graduate Studies

Dr. Bruce McLeod      Bruce McLeod      1-20-99  
Signature      Date

## STATEMENT OF PERMISSION TO USE

In presenting this thesis in partial fulfillment of the requirements for a doctoral degree at Montana State University-Bozeman, I agree that the Library shall make it available to borrowers under the rules of the Library. I further agree that copying of this thesis is allowable only for scholarly purposes, consistent with "fair use" as prescribed in the U.S. Copyright Law. Requests for extensive copying or reproduction of this thesis should be referred to University Microfilms International, 300 North Zeeb Road, Ann Arbor, Michigan 48106, to whom I have granted "the exclusive right to reproduce and distribute my dissertation in and from microform along with the non-exclusive right to reproduce and distribute my abstract, in whole or in part."

Signature

Loenece P. Brown

Date

1/7/99

## ACKNOWLEDGEMENTS

I would first like to thank my advisor, Dr. Anthony Demetriades, for his encouragement and guidance over the last 6 years. His often subtle suggestions have provoked my technical imagination, desire to learn, and determination for understanding to a level far beyond what I could have achieved on my own. Through my graduate program, I have gained both a colleague and friend.

I have enjoyed the many enlightening technical discussions with members of the Fluid Mechanics Laboratory at NASA Ames Research Center. In particular, I would like to thank Jim Laub for his moral support and the encouragement to pursue a Ph.D., as well as Lyn King for the invaluable assistance with the numerical calculations (and general understanding of Fluid Mechanics!).

The members of my graduate committee, Drs. Frank Albin, Jay Conant, Alan George, Ken Bowers, and Anthony Demetriades, have all had a profound influence on my ability to reason, both mathematically and physically, in the Engineering Sciences. The helpful comments they have provided to the manuscript are also acknowledged. Many thanks to Terry Kennedy, Dana Aughney, and Barbara Valdez in the Mechanical Engineering office, who have kept things smooth, even when they were not.

Last, and most important, I would like to thank my wife, RaKyel, for her unwavering love and support. While giving up countless weekends, evenings, and vacations, she has always encouraged me to strive for excellence. Words could not describe the amount of effort, which was often unrecognized, that she has invested into my education. This work is as much hers as it is mine.

This work has been funded by a GSRP Fellowship from NASA-AMES, thanks in large part to the efforts of Sanford Davis and Jim Laub.

## TABLE OF CONTENTS

LIST OF TABLES

LIST OF FIGURES

NOMENCLATURE

ABSTRACT

CHAPTER 1 INTRODUCTION .....	1
1.1 Background .....	1
1.1.1 Applications of Transition Experiments.....	1
1.1.2 Sources of Free-stream Noise in a Supersonic Wind Tunnel .....	3
1.1.3 Effects of Free-stream Noise on Transition.....	4
1.1.4 Organization of the Literature Review .....	6
1.2 Supersonic Boundary Layer Transition Mechanisms .....	6
1.2.1 Boundary Layer Stability Prediction.....	9
1.2.2 Boundary Layer Transition Prediction .....	11
1.2.3 Heat-Transfer Mechanisms in Stability and Transition.....	14
1.3 State of the Art in Quiet Wind Tunnels .....	17
1.3.1 Boundary Layer Development on a Supersonic Nozzle.....	19
1.3.2 Nozzle Design Features for Laminar Flow Control and Noise Reduction.....	20
1.3.3 Observed Temperature Effects on Nozzle Boundary Layers .....	21
1.4 Purpose of This Investigation.....	22
CHAPTER 2 APPROACH.....	28
2.1 Wind tunnel and Nozzle Configuration .....	28
2.1.1 Wind tunnel.....	28
2.1.2 Nozzle Modifications .....	29
2.2 State of the Unheated Nozzle Boundary Layer .....	30
2.3 Scope of the Surface Heating Investigation .....	31
CHAPTER 3 COMPUTATIONAL METHODS.....	36
3.1 Navier-Stokes Solution .....	37
3.1.1 OVERFLOW Description.....	37
3.1.2 Grids .....	40
3.1.3 Initial Conditions and Boundary Conditions .....	42
3.2 Two-dimensional Boundary Layer Solution .....	43
3.3 Stability Computations.....	45
3.3.1 General method.....	45
3.3.2 Görtler instability .....	49

3.3.3	Transition prediction .....	52
3.3.4	Numerical method .....	53
CHAPTER 4	NUMERICAL RESULTS .....	57
4.1	Mean-flow Results .....	57
4.1.1	Navier-Stokes Solution .....	57
4.1.2	Mean-flow on Nozzle Contoured Surface .....	59
4.2	Boundary Layer Stability on the Nozzle Floor .....	65
4.2.1	Görtler Instability .....	66
4.2.2	First-mode Tollmien-Schlichting Instability .....	71
4.3	Numerical Accuracy of the Solutions .....	76
4.3.1	Navier-Stokes Solution .....	76
4.3.2	Boundary Layer Solutions .....	79
CHAPTER 5	EXPERIMENTAL MEASUREMENTS .....	97
5.1	Unsteady Measurement Techniques .....	98
5.1.1	Sensor .....	98
5.1.2	Electronic Circuit .....	99
5.1.3	Data Reduction .....	100
5.2	Interpretation of the DPP Signal .....	102
5.2.1	Thermodynamic Relations .....	102
5.2.2	Treatment of Boundary Layer Mean-Flow .....	105
5.3	MEP Recordings .....	106
5.3.1	Location of MEP .....	107
5.3.2	RMS progression .....	109
5.3.3	Time Series .....	111
5.3.4	Turbulent Intermittency .....	112
5.3.5	Fourier Spectrum Analysis .....	114
5.3.6	Amplification Rates .....	116
5.4	Free-stream Disturbance Environment .....	119
CHAPTER 6	DISCUSSION .....	139
6.1	Comparison of Theory and Experiment .....	139
6.1.1	Unheated Nozzle Surface .....	139
6.1.2	Heated Nozzle .....	142
6.1.3	Steady Disturbances .....	144
6.2	The Relation of Heat-Transfer to Instability and Transition Suppression .....	144
6.2.1	Effect on Receptivity and Bypass .....	145
6.2.2	Effect on Growth of Infinitesimal Disturbances .....	149
6.3	Comparison to other facilities .....	151
6.3.1	Summary of Transition Delay .....	151
6.3.2	Postulated Mechanisms .....	153
6.4	Suggestions for Future Work .....	158
6.4.1	Theoretical Predictions .....	158



6.4.2 Experimental Measurements.....	159
CHAPTER 7 CONCLUSIONS .....	163
APPENDICES .....	167
APPENDIX A: DOCUMENTATION FOR ANALOG TAPE RECORDINGS .....	168
APPENDIX B: COMPUTATION OF AMPLIFICATION RATES FROM EXPERIMENTALLY DETERMINED POWER SPECTRA .....	181
APPENDIX C: DIGITAL TECHNIQUES FOR INTERMITTENCY COMPUTATION .....	190
REFERENCES.....	212

## LIST OF TABLES

Table 2-1. Matrix of flow conditions for the surface heating investigation. Theoretical predictions are executed for the same. ....	33
Table 3-1. Geometric grid parameters of the Navier-Stokes solution for the MSU-SWT nozzle. ....	55
Table 4-1. Convergence parameters in two-dimensional Navier-Stokes computation. $Re'_{\infty}=5.2 \times 10^6/m$ , All solutions stopped at 3500 iterations. ....	82
Table 6-1. Comparison of heat transfer effect between three facilities. ....	161

## APPENDIX TABLES

Table A-1. Documentation for Analog Data Recordings at MEP, $Re'_{\infty}=5.2 \times 10^6/m$ , Unheated nozzle. ....	171
Table A-2. Documentation for Analog Data Recordings at MEP, $Re'_{\infty}=5.2 \times 10^6/m$ , Unheated nozzle. ....	173
Table A-3. Documentation for Analog Data Recordings at MEP, $Re'_{\infty}=5.2 \times 10^6/m$ , Unheated nozzle. ....	174
Table A-4. Documentation for Analog Data Recordings at MEP, $Re'_{\infty}=5.2 \times 10^6/m$ , Unheated nozzle. ....	176
Table A-5. Documentation for Analog Data Recordings at MEP, $Re'_{\infty}=5.2 \times 10^6/m$ , Unheated nozzle. ....	177
Table A-6. Documentation for Analog Data Recordings at MEP, $Re'_{\infty}=5.2 \times 10^6/m$ , Unheated nozzle. ....	179
Table A-7. Documentation for Analog Data Recordings at MEP, $Re'_{\infty}=5.2 \times 10^6/m$ , Unheated nozzle. ....	180
Table C-1. Intermittency range and threshold values for selected waveform records. ....	199
Table C-2. Characteristic time scales. ....	200

## LIST OF FIGURES

Figure 1-1. Unsteady disturbances found in a supersonic wind tunnel. Acoustic radiation from group (c) is the most common cause of premature transition in a supersonic wind tunnel model. Adapted from (Morkovin 1959). .....	24
Figure 1-2. Disparity of transition experiments on a $10^\circ$ cone between the best "conventional" wind tunnels, and flight-data. Quiet wind tunnel data is shown for comparison. Graph adapted from (Dougherty and Fisher 1982). .....	25
Figure 1-3. System portrait of roads to wall turbulence. Reproduced from (Morkovin 1991). .....	26
Figure 1-4. Effect of wall temperature on transition near the throat. Adapted from (Demetriades 1981a, Demetriades 1992a). .....	27
Figure 1-5. Illustration of the "quiet test core" in a low-disturbance supersonic wind tunnel. Picture of Mach 3.5 Quiet tunnel at NASA-Langley adapted from (Beckwith and Miller 1990). .....	27
Figure 2-1. Section view of the MSU-SWT Mach 3 wind tunnel showing components of the settling chamber, contraction, and nozzle. ....	34
Figure 2-2. Schematic of the MSU-SWT 2-D Mach 3 Nozzle. (Nozzle length is $L=38.48$ cm) .....	34
Figure 2-3. Heater configuration and thermocouple locations .....	35
Figure 2-4. Transition map in the MSU-SWT nozzle @ $20.^\circ\text{C}$ with data range of the present fluctuation measurements. ....	35
Figure 3-1. Grid used in the two-dimensional Navier-Stokes computations: coarse-grid shown ( $140 \times 41$ ), every grid line in $j$ -direction, and every other grid line in $k$ -direction. ....	55
Figure 3-2. Grid spacing in the wall-normal direction ( $k$ ) at the nozzle throat ( $x=0$ ). .....	55
Figure 3-3. Grid spacing in the streamwise direction ( $j$ ) on the nozzle surface. ....	56
Figure 3-4. Görtler vortices in the boundary layer of a concave wall. Adapted from (Saric 1994). .....	56
Figure 4-1. Normalized static pressure at boundary layer edge predicted by the Navier-Stokes code. ....	82

Figure 4-2. Pressure gradient parameter computed in the boundary layer solution.....	83
Figure 4-3. Streamwise surface temperature distribution for heated and unheated nozzle condition. Symbols indicate thermocouple measurements. ....	83
Figure 4-4. Spanwise uniformity of surface temperatures. Symbols indicate thermocouple measurements. ....	84
Figure 4-5. Calculated heat flux from 2D boundary layer code using measured temperature distributions. ....	84
Figure 4-6. Mean-flow profiles for normalized velocity $U/U_e$ and static temperature $T/T_e$ . $Re'_\infty=5.2\times 10^6/m$ , heated condition is $(T_w/T_o)_{x=0}=1.13$ . ....	85
Figure 4-7. Mean-flow profiles for normalized velocity $U/U_e$ and static temperature $T/T_e$ . $Re'_\infty=6.2\times 10^6/m$ , heated condition is $(T_w/T_o)_{x=0}=1.22$ . ....	86
Figure 4-8. Boundary layer thickness and integral properties with and without surface heating. ....	87
Figure 4-9. Shape factor $H_{12}$ progression with and without surface heating. ....	87
Figure 4-10. Local roughness Reynolds number through the throat region using the maximum peak to valley differential (PVD) for roughness height. $k=1.2\mu m$ . ....	88
Figure 4-11. Variation in Görtler number based on momentum thickness with and without surface heating. ....	88
Figure 4-12. Amplification rate $\sigma$ of the steady Görtler instability as a function of spanwise wavelength, $\lambda_z$ . Arrows indicate the point at which $\lambda_z=2\delta$ with heat (solid) and without heat (dash). Streamwise position near most unstable point ( $x/L=0.500$ ). ....	89
Figure 4-13. Computed $N$ -factors of the steady Görtler instability for the spanwise wavelength of largest growth at nozzle exit. ....	89
Figure 4-14. Eigenfunctions of the Görtler instability. $Re'_\infty=6.2\times 10^6/m$ , $x/L=0.729$ , $\lambda_z=0.255$ cm. All eigenfunctions are normalized by $\hat{u}_{max}$ . ....	90
Figure 4-15. Amplification rate $-\alpha_i$ of the unsteady Görtler instability, as a function of dimensionless frequency, $F$ . Near most unstable wavelength, $\beta=0.7$ (see Figure 4-12). ....	90

- Figure 4-16. Spectra of "maximum" amplification rates  $-\alpha_i$  for first-mode instability with and without surface heating. Nozzle exit ( $x/L=1$ ), wave-angle varied to maximize  $-\alpha_i$  for each frequency. .... 91
- Figure 4-17. Eigenfunctions of the first-mode TS instability with and without surface heating.  $Re'_\infty=6.2\times 10^6/m$ ,  $x/L=1.0$ ,  $f=5$  kHz,  $\phi=68^\circ$ . All eigenfunctions are normalized by  $|\hat{u}|_{\max}$  ..... 91
- Figure 4-18. Effect of heating on amplification rate  $-\alpha_i$  beyond nozzle exit. Adiabatic wall specified for  $x/L>1$ , wave-angle varied to maximize  $-\alpha_i$  for each frequency. .... 92
- Figure 4-19. Comparison of adiabatic and unheated conditions on amplification rate  $-\alpha_i$  beyond nozzle exit. Adiabatic wall specified for  $x/L>1$ , wave-angle varied to maximize  $-\alpha_i$  for each frequency. .... 92
- Figure 4-20. Progression of  $D(\rho DU)$  profiles with and without surface heating in the nozzle. Adiabatic wall specified for  $x/L>1$ . Subscript  $( )_\eta$  denotes derivative with respect to normal coordinate  $\eta$ . Subscript  $( )_e$  denotes edge quantity. .... 93
- Figure 4-21. Residual history for 2D Navier-Stokes computation,  $P_o=350$  mmHg,  $T_o=38^\circ\text{C}$ ,  $Re'_\infty=3.28\times 10^6/m$ ,  $140\times 41$  grid,  $\Delta t=1$ ,  $CFL_{\min}=5$ . .... 94
- Figure 4-22. Iteration convergence of floor boundary layer in 2D Navier-Stokes computation. Conditions of Figure 4-21, matrix dissipation, 3 levels FMG. .... 94
- Figure 4-23. Grid dependence of boundary layer on contoured surface: 2D Navier-Stokes computation.  $P_o=500$  mmHg,  $T_o=21^\circ\text{C}$ ,  $Re'_\infty=5.2\times 10^6/m$ . .... 95
- Figure 4-24. Boundary layer conditions from Navier-Stokes solution (top) Edge Mach number, (bottom) displacement thickness. .... 95
- Figure 4-25. Convergence of boundary layer solution for derivative computations.  $Re'_\infty=5.2\times 10^6/m$ ,  $(T_w/T_o)_{x=0}=1.13$ ,  $x/L=1.0$  ..... 96
- Figure 5-1. Schematic of the dynamic pitot probe (DPP) consisting of an ultraminiature Kulite mounted on a probe sting. (Probe reflection off of nozzle surface shows polishing quality) ..... 123
- Figure 5-2. Recording and playback circuit for unsteady measurements with the dynamic pitot probe (DPP). .... 123

- Figure 5-3. Typical power spectra with and without electronic noise. Conditions are from  $Re'_\infty=5.2\times 10^6/m$ , Unheated. (top) "robust" signal, (bottom) "weak" signal with low signal to noise ratio. .... 124
- Figure 5-4. Amplitude envelope for fluctuations sensed by a dynamic pitot probe in a supersonic boundary layer. .... 125
- Figure 5-5. Technique to determine maximum energy point (MEP) within the boundary layer. Tic-marks indicate the MEP. Each trace is a different streamwise ( $x$ ) position on the nozzle. .... 125
- Figure 5-6. Location of maximum energy point (MEP) within the boundary layer at  $Re'_\infty=5.2\times 10^6/m$  with and without surface heating. Flagged symbol indicates measurements by Demetriades (1996) at the same stagnation conditions. .... 126
- Figure 5-7. Location of maximum energy point (MEP) within the boundary layer at  $Re'_\infty=6.2\times 10^6/m$  with and without surface heating. Flagged symbols indicate measurements by Demetriades (1996) at the same stagnation conditions. .... 126
- Figure 5-8. Wideband pitot pressure fluctuations at the maximum energy point (MEP) with and without surface heating. Computed by integrating averaged power spectra from 156 Hz to 320 kHz. Electronic noise subtracted in the square. .... 127
- Figure 5-9. Wideband velocity fluctuations for  $Re'_\infty=5.2\times 10^6/m$ . Calculated with equation 5-5 using mean-flow computed from boundary layer theory. Error bars based on total variation in MEP location ( $y/\delta$ ) of 15%. .... 127
- Figure 5-10. Progression of sample waveforms at maximum energy point (MEP).  $Re'_\infty=5.2\times 10^6/m$ , Unheated. .... 128
- Figure 5-11. Progression of sample waveforms at maximum energy point (MEP).  $Re'_\infty=5.2\times 10^6/m$ , Heated  $(T_w/T_o)_{x=0}=1.13$ . .... 129
- Figure 5-12. Progression of sample waveforms at maximum energy point (MEP).  $Re'_\infty=6.2\times 10^6/m$ , Unheated. .... 130
- Figure 5-13. Progression of sample waveforms at maximum energy point (MEP).  $Re'_\infty=6.2\times 10^6/m$ , Heated  $(T_w/T_o)_{x=0}=1.22$ . .... 131
- Figure 5-14. Intermittency technique applied to sample waveform ( $Re'_\infty=5.2\times 10^6/m$ , Unheated,  $x/L=0.949$ );  $\gamma$ =Intermittency;  $C$ =Threshold criterion. .... 132

Figure 5-15. Streamwise progression of intermittency with and without surface heating .....	132
Figure 5-16. Streamwise progression of power spectral density at the maximum energy point with and without surface heating. $Re'_{\infty}=5.2 \times 10^6/m$ . Electronic noise subtracted in the square. ....	133
Figure 5-17. Streamwise progression of power spectral density at the maximum energy point with and without surface heating. $Re'_{\infty}=6.2 \times 10^6/m$ . Electronic noise subtracted in the square. ....	134
Figure 5-18. Dimensionless frequency at the maximum spectral intensity. Maxima computed from smoothed spectra. ....	135
Figure 5-19. Comparison of fluctuation rms amplitude spectrum with and without surface heating at the first measurement location. ....	135
Figure 5-20. Smoothed power spectral density of Figure 5-16. $Re'_{\infty}=5.2 \times 10^6/m$ . Polynomial smoothing procedure used with $10^{\text{th}}$ -order polynomial in frequency and $7^{\text{th}}$ -order polynomial in the streamwise direction. ....	136
Figure 5-21. Comparison of spatial amplification rates based on $p_p'_{rms}$ at selected Fourier components. $Re'_{\infty}=5.2 \times 10^6/m$ with and without surface heating. Spatial amplification rates nondimensionalized with viscous length scale $l^*$ . ....	137
Figure 5-22. Comparison of spatial amplification rates based on $u'_{rms}$ at selected Fourier components. $Re'_{\infty}=5.2 \times 10^6/m$ with and without surface heating. Spatial amplification rates nondimensionalized with viscous length scale $l^*$ . ....	138
Figure 6-1. Comparison of spatial amplification rates ( $-\alpha_{i,l^*}$ ) between the experiment and linear stability theory (LST) for traveling Görtler modes at $Re'_{\infty}=5.2 \times 10^6/m$ with and without surface heating. Heated condition is $(T_w/T_o)_{x=0}=1.13$ . ....	162

#### APPENDIX FIGURES

Figure B-1. Example raw spectra progression. $Re'_{\infty}=5.2 \times 10^6/m$ , Unheated Nozzle. ....	185
---	-----

Figure B-2. Variations of a smoothed curve in the frequency domain with polynomial order $n_f$ .....	185
Figure B-3. Variations of a smoothed curve in the spatial domain with polynomial order $n_x$ .....	186
Figure B-4. Spectra progression with smoothing using polynomials ( $n_f=10$ ) in the frequency domain only.....	186
Figure B-5. Spectra progression with smoothing using polynomials ( $n_x=7$ ) in the spatial domain only.....	187
Figure B-6. Spatial derivative $\partial A/\partial x$ computed from spectra smoothed only in the spatial domain (spectra progression in Figure B-5).....	187
Figure B-7. Global variance of smoothed spectra with different polynomial degrees in frequency domain ( $n_f$ ).....	188
Figure B-8. Global variance of spatial derivatives ( $\partial A/\partial x$ ) with different polynomial degrees in frequency domain ( $n_f$ ).....	188
Figure B-9. Global variance of smoothed spectra with different polynomial degrees in spatial domain ( $n_x$ ). .....	189
Figure B-10. Global variance of spatial derivatives ( $\partial A/\partial x$ ) with different polynomial degrees in spatial domain ( $n_x$ ).....	189
Figure C-1. Intermittency computation using a peak-to-peak detector, $P_o=500$ mmHg, $T_o=21$ °C, Unheated Nozzle, $x/L=0.949$ .....	202
Figure C-2. Intermittency computation using a peak-to-peak detector, $P_o=595$ mmHg, $T_o=16$ °C, Unheated Nozzle, $x/L=0.942$ .....	202
Figure C-3. General digital high-pass filter characteristics.....	203
Figure C-4. Attenuation Characteristics of different IIR and FIR filter types. Nyquist frequency $f_N=320$ kHz, Cutoff frequency, $f_{cut}=15$ kHz.....	204
Figure C-5. Intermittency computation using a 20 kHz filtered mean-square detector, $P_o=500$ mmHg, $T_o=21$ °C, Unheated Nozzle, $x/L=0.949$ .....	205
Figure C-6. Intermittency computation using a 20 kHz filtered mean-square detector, $P_o=595$ mmHg, $T_o=16$ °C, Unheated Nozzle, $x/L=0.942$ .....	206



Figure C-7. Intermittency computation using a 20 kHz filtered mean-square detector, $P_o=500$ mmHg, $T_o=21$ °C, Heated Nozzle, $(T_w/T_o)_{x=0}=1.13$ , $x/L=0.949$ .	207
Figure C-8. Intermittency computation using a 20 kHz filtered mean-square detector, $P_o=595$ mmHg, $T_o=16$ °C, Heated Nozzle, $(T_w/T_o)_{x=0}=1.22$ , $x/L=0.943$ .	208
Figure C-9. Intermittency sensitivity to threshold values. Conditions for curves are $P_o=500$ mmHg, $T_o=21$ °C, Unheated Nozzle. (PP) Peak-to-peak detector, (MS) Mean-square detector. Arrows indicate range of "realistic" intermittency by visual inspection of the waveforms, detector, and indicator functions.	209
Figure C-10. Filtered mean-square detector function applied to electronic noise recording.	210
Figure C-11. PDF plots with 100 waveforms averaged.	211

## NOMENCLATURE

<u>Symbol</u>	<u>Description</u>
$A$	amplitude of an instability
$A_o$	amplitude of an instability at the neutral stability point
$c_r$	phase speed of an instability wave
$e$	voltage -or- exponential
$f$	physical frequency of disturbance (kHz)
$F$	Dimensionless disturbance frequency (normalized on a convective scale) $F=(2\pi v_e/U_e^2)f$
$G$	Görtler number based on a generic reference length
$G_\theta$	Görtler number based on momentum thickness, $\theta$ . $G_\theta = \frac{U_e \theta}{v_e} \left( \frac{\theta}{r_c} \right)^{1/2}$
$h$	height of the nozzle throat $h=1.799$ cm
$H_{12}$	Shape factor, $H_{12}=\delta^*/\theta$
$i$	$(-1)^{1/2}$
$j$	grid index in the streamwise direction
$k$	maximum peak-to-valley roughness height, <i>or</i> grid index normal to the wall
$L$	nozzle length (throat to test section entrance) $L=38.48$ cm.
$l^*$	viscous length scale, $l^*=(v_e s/U_e)^{1/2}$
$M$	Mach number
$n$	time-stepping index
$N$	$N$ -factor, $N=\ln(A/A_o)$
$P$	static pressure

$p'$	disturbance state static pressure
$P_o$	stagnation pressure
$P_p$	pitot pressure: total pressure behind a normal shock
$p_p'$	disturbance state pitot pressure
$Q$	vector of unknowns in the Navier-Stokes solution —or— a general basic state flow quantity
$q'$	general disturbance state quantity
$q_w$	heat flux at the wall (+ into the boundary layer)
$r_c$	local radius of curvature
$Re$	Reynolds number
$Re_k$	roughness Reynolds number based on local conditions from a smooth-wall solution at the tip of the roughness element, $Re_k = U_k k / \nu_k$
$Re_\theta$	Reynolds number based on momentum thickness $\theta$
$Re_{\Delta x}$	Reynolds number based on length of quiet flow: Quiet-flow Reynolds number
$Re'_\infty$	Unit Reynolds number based on free-stream conditions at Mach 3, $Re'_\infty = U_\infty / \nu_\infty$
$s$	arc-length, ( $s=0$ @ start of boundary layer computation)
$S_u$	velocity sensitivity coefficient of the dynamic pitot probe
$t$	time
$T$	mean temperature
$T'$	disturbance state temperature
$T_o$	stagnation temperature

$T_o'$	disturbance state stagnation temperature
$U, V, W$	mean velocity in the $x, y, z$ directions, respectively
$u', v', w'$	disturbance velocity in the $x, y, z$ directions, respectively
$x$	streamwise coordinate ( $x=0$ @ nozzle throat)
$y$	vertical distance from the wall ( $y=0$ @ wall)
$y^+$	turbulent law-of-the-wall variable
$z$	spanwise distance from the nozzle centerline ( $z=0$ @ centerline)
$\alpha$	dimensionless streamwise component of the wavenumber
$\beta$	dimensionless spanwise component of the wavenumber
$\beta^*$	spanwise component of the wavenumber ( $=l^*\beta$ )
$\beta_H$	pressure gradient parameter
$\delta$	boundary layer thickness, $\delta=y$ @ $U/U_e=0.99$
$\delta^*$	displacement thickness, $\delta^* = \int_0^\infty \frac{\rho}{\rho_e} \left( \frac{U}{U_e} - 1 \right) dy$
$\lambda$	disturbance wavelength
$\lambda_z$	disturbance wavelength in spanwise direction, $\lambda_z=2\pi/\beta$
$\theta$	momentum thickness, $\theta = \int_0^\infty \frac{\rho U}{\rho_e U_e} \left( \frac{U}{U_e} - 1 \right) dy$
$\gamma$	turbulent intermittency <i>or</i> ratio of specific heats
$\phi$	disturbance wave-angle, $\phi=\tan^{-1}(\alpha_r/\beta)$
$\rho$	density
$\sigma$	amplification rate of steady Görtler instability
$\mu$	dynamic viscosity

$\nu$	kinematic viscosity, $\nu = \mu/\rho$
$\omega$	dimensionless circular frequency of the disturbance, $\omega = 2\pi f(l^*/U_e)$
$\xi$	transformed streamwise coordinate in the computational plane
$\eta$	dimensionless normal coordinate, $\eta = y/l^*$
$\eta_{BL}$	transformed normal coordinate for boundary layer solution

### Subscripts

<u>Symbol</u>	<u>Description</u>
$()_{aw}$	local adiabatic conditions at the nozzle block surface
$()_e$	conditions at the edge of the boundary layer; represents a local free-stream quantity
$()_i$	imaginary component of a complex number
$()_N$	value at neutral point ( $\alpha_i = 0$ )
$()_r$	real component of a complex number.
$()_T$	value at transition onset
$()_w$	local wall conditions
$()_\infty$	conditions based on tunnel core flow Mach number
$()_{rms}$	root-mean-square value

### Superscripts

$()$	instantaneous flow quantity (basic state + disturbance state)
$()'$	disturbance state quantity

( $\wedge$ ) disturbance eigenfunction

Acronyms

BW	Beam-Warming
DAC	digital to analog conversion
CFD	computational fluid dynamics
LFC	laminar flow control
LST	linear stability theory
MEP	maximum energy point
MSU	Montana State University
PSE	parabolized stability equations
SWT	Supersonic wind tunnel
TS	Tollmien-Schlichting

## ABSTRACT

Acoustic fluctuations that originate from transitional and turbulent boundary layers in a supersonic wind tunnel limit the capabilities of ground test facilities for boundary layer transition research and testing. The present work explores boundary layer stability and transition with and without surface heating on one contoured wall of a low-disturbance Mach 3 two-dimensional wind tunnel at Montana State University.

The throat area of the lower contoured surface was heated to a steady state temperature of 13% and 22% over the stagnation temperature at unit Reynolds numbers of  $5.2 \times 10^6/\text{m}$  and  $6.2 \times 10^6/\text{m}$ , respectively. Boundary layer measurements with a small, fast-response, pitot probe were used to characterize fluctuation magnitude, frequency content, and the rate of amplification with and without surface heating. The effect of surface heating was to reduce the amplitude of a low frequency disturbance at all streamwise positions. Suppressing this low frequency activity caused turbulent bursting to be moved downstream, thereby increasing the extent of laminar flow to nearly the entire nozzle length. Predictions with linear stability theory showed that heat has a mild stabilizing effect on Görtler vortices, and first-mode Tollmien-Schlichting waves could be suppressed with a proper heating distribution by moving the neutral point downstream and reducing the subsequent amplification rates. However, the  $e^N$  method with linear stability theory completely failed to predict the observed transition in the nozzle boundary layer due to unsteady oscillations, even in the case without surface heating. Calculations of the mean-flow also showed that natural cooling (heat followed by cooling) and roughness arguments do not appear to explain the observed stability events.

The experiment and theory show at least two different paths to turbulence suppression by heating the surface of a supersonic nozzle. (1) The experiment demonstrates that heat suppresses a bypass mechanism triggered by receptivity events near and possibly upstream of the nozzle throat. (2) The computations show that a proper heating distribution can also be used to suppress the growth of linear instabilities in the nozzle if bypass were not present.

## CHAPTER 1

### INTRODUCTION

#### 1.1 Background

As design margins for modern supersonic and hypersonic flight vehicles become tighter, the fidelity of engineering predictions for thermal and aerodynamic loading become increasingly important. Since the magnitudes of skin friction and heat transfer depend heavily on whether the boundary layer is laminar or turbulent, the natural state of the boundary layer over the vehicle surface becomes a “first-order” variable in the design process. Yet, the location and extent over which boundary layer transition occurs is often the largest source of uncertainty in sub-system performance. Furthermore, if the physics of the boundary layer transition process are well understood, then control becomes a reality, with potentially high pay-off.

##### 1.1.1 Applications of Transition Experiments

Some estimates have indicated that if laminar flow can be maintained on the wings of a large commercial transport, the reduction in skin-friction drag would give as much as 25% savings in fuel (Reed et al. 1996). This has obvious implications for transport range, payload economy, and emissions control to the environment. A recent numerical study by King et al. (1998) has also shown that the location and extent of boundary layer



transition has a significant influence on both lift and drag of supercritical airfoils by changing the location of the shock-wave, and the subsequent shock-boundary layer interaction. This is an important finding, since the transition location is usually prescribed a priori, rather than computed from physical principles with the flow-field solution. Perhaps the most severe consequences for accurate transition prediction are found in the heating requirements for thermal protection systems (TPS) on hypersonic re-entry vehicles like the Space Shuttle (Olynick and Tam 1997) and the Lockheed X-33 technology demonstrator. If the current design predictions for boundary layer transition on the X-33 were to be exceeded, "the increased heating would exceed the TPS limits." (Thompson et al. 1998) An overly conservative design increases the vehicle weight, decreases payload capacity, and changes the allowable flight trajectories. The goal of single-stage to orbit also becomes more difficult.

Although there has been much progress in modeling boundary layer transition (Reshotko 1997a), there are still many shortcomings that prevent transition prediction and control based on first-principles, particularly for three-dimensional flows, and elevated disturbance environments; the problem is magnified at supersonic and hypersonic speeds. Further progress can only be achieved with wind tunnel experiments of sufficient quality to use for model validation (Haynes et al. 1996), and the conclusive identification of relevant flow physics. The basic component to these experiments is a wind tunnel that has a high-quality flow field in which disturbances are below various threshold values similar to free-flight conditions. These low-disturbance wind tunnels in the supersonic

and hypersonic regime are termed "quiet" wind tunnels for their low levels of free-stream noise.

### 1.1.2 Sources of Free-stream Noise in a Supersonic Wind Tunnel

A review by Morkovin (1959) discusses the various sources of disturbances found in wind tunnels (Figure 1-1)<sup>1</sup>. The unsteady disturbances can be categorized into three unique modes that can exist independent of one another in a compressible flow. Vorticity (turbulence) and entropy (temperature spottiness) modes are convected disturbances that propagate along streamlines, and are traceable to conditions upstream of the nozzle throat. The third type of disturbance is an acoustic mode, whose intensity radiates across streamlines along local Mach lines. Vorticity and entropy modes can be mitigated with proper stilling tank design and screen arrangements located downstream of the classic disturbance generators listed in the left of Figure 1-1, and just upstream of the contraction. Additionally, Laufer (1961) showed that above about Mach 2.5, the acoustic disturbances dominate the free-stream flow field and the convected disturbances are damped due to the high accelerations and flow-stretching through the nozzle.

The acoustic disturbances are composed of fluctuations that originate at the wall due to a localized "effective" displacement of the boundary layer. In the case of wall roughness and waviness, the surface geometry produces a local pressure perturbation (Mach-wave) that emanates from a fixed location, and any unsteadiness in the boundary layer causes the Mach-wave to shiver, so that this wrinkled Mach-wave displaces back

---

<sup>1</sup> Figures and tables are located at the end of each chapter.

and forth relative to a fixed observer. As boundary layer transition sets in, discrete turbulent eddies form that protrude above the surface of the boundary layer. Each of these eddies is capped by a weak, unsteady, conical shock wave that moves with the speed of the eddy (Laufer 1964). As one approaches hypersonic speeds discrete turbulent bursts are even observed in the free-stream as eddy-Mach-waves convect past a stationary probe (Stainback et al. 1974, Wilkinson et al. 1994, Schnieder and Haven 1995). Recently, Wilkinson (1997), and Brogan and Demetriades (1998) have also shown that unstable activity in the boundary layer can interact with the stream to produce pressure perturbations before the formation of turbulent bursting in the wall boundary layer. As the Mach number increases in the core flow, the effect of perturbations in the inviscid surface are amplified proportional to  $M^2$  (Laufer 1961).

### 1.1.3 Effects of Free-stream Noise on Transition

Pate and Schueler (1969) and Pate (1980) clearly demonstrated that the transition process on a model can occur at lower Reynolds numbers when acoustic disturbances originating from eddy-Mach-waves in a transitional and turbulent boundary layer impinge on a model. These acoustic waves act as a forcing function (Mack 1975) that, at the proper frequencies, can prematurely excite instabilities within the model boundary layer causing the layer to break down to turbulence. The leading edge region is particularly susceptible to the adverse effects of wind tunnel noise.

Dougherty and Fisher (1982) also made a direct comparison of the Reynolds number at transition onset ( $Re_T$ ) in wind tunnel and flight experiments at identical conditions with the same  $10^\circ$  sharp cone. Figure 1-2 shows the results of Dougherty and Fisher,

supplemented by flight data at higher Mach numbers as reported in Beckwith et al. (1983)<sup>2</sup>. With increasing Mach number, Figure 1-2 graphically illustrates the large disparity between supersonic transition experiments conducted in conventional wind tunnels and those of free flight. The noise characteristics of these conventional supersonic wind tunnels are typically more than an order of magnitude above that found in free-flight, primarily because of the acoustic radiation from the turbulent boundary layer on the tunnel walls (recall radiated noise increases with  $M^2$ ). Moreover, when the same experiment is conducted in a quiet wind tunnel with laminar wall boundary layers, noise levels approach those of free-flight, and  $Re_T$  increases to flight-values. The "quiet tunnel data" (Beckwith et al. 1983, Creel et al. 1985, Chen 1993) in Figure 1-2 was acquired again on a  $10^\circ$  cone in the two-dimensional Langley Mach 3.5 Pilot Quiet Tunnel (cone  $M_e=3.33$ ) with only the apex of the cone subject to a low noise environment. Higher  $Re_T$  values were limited by the model size and tunnel conditions; it is still possible that if larger runs of low-noise flow were permitted on the model,  $Re_T$  would continue to increase.

It is also important to realize that the increased noise levels not only move transition forward in general, but they also modify parametric effects so that the transition test in the conventional tunnel has no relevance to free-flight conditions.

---

<sup>2</sup> This flight data is only about half of a larger data set also reported by Beckwith (1975). The reason for omitting these points is not known, although the latter is far outside the general cluster of data for  $M_e < 5$ . The conditions and  $Re_T$  values of the complete data set are documented in (Schneider 1998b).

Therefore, if one is to conduct meaningful experiments dealing with boundary-layer transition on a wind tunnel model it is essential that the boundary layer growing along the wind tunnel nozzle itself remains laminar, to the extent that Mach waves emanating downstream of transition in the latter boundary layer do not impinge on the model. Because of this linkage between the boundary-layer turbulence and the free-stream disturbances, understanding the nozzle boundary layer is a prerequisite for attacking the free-stream disturbance problem systematically, and for designing "quiet" wind tunnels.

#### **1.1.4 Organization of the Literature Review**

The purpose of this thesis is to first, to understand more fully the mechanism(s) of boundary layer instability and transition on the wind tunnel walls and second, to explore how surface heating can be used as a design technique for delaying those instability mechanism(s) which cause transition in the nozzle boundary layer. In the remainder of this chapter, the elements of the transition process are first reviewed, emphasizing the mechanisms preceding transition. Then the current state of the art in quiet wind tunnels is discussed. Finally, the objectives of the present research are presented.

### **1.2 Supersonic Boundary Layer Transition Mechanisms**

The evolution from a laminar to turbulent boundary layer is a process that begins with disturbances at the boundaries (i.e. surface and free-stream edge) of the layer. The Navier-Stokes equations dictate that with a proper match in scale and frequency, these disturbances will be ingested into the layer, then be naturally amplified by the conditions in the layer without the aid of external forcing. When disturbances *in the boundary layer*

grow to a certain point, a localized region of turbulence appears. With increasing distance, more turbulent "spots" appear and merge together, until a fully turbulent layer is achieved; that is, the production of turbulence is self-sustained, stable, and statistically stationary. Morkovin (1991) developed a "system portrait of roads to wall turbulence" reproduced here as Figure 1-3. The details of this schematic are still not complete, and some still poorly understood, but the portrait covers the major categories of the transition problem.

The mechanism(s) by which the disturbances like sound, vorticity, and roughness can be converted to free-waves in the boundary layer ("eigenmodes") is termed receptivity, and, as illustrated in Figure 1-3, it encompasses and influences the entire transition process. First, receptivity provides the crucial information for the initial amplitude, phase, and frequency at the inception of the primary instability. Second, distributed receptivity recognizes the boundary layer as a truly open system, to provide the boundary conditions for the disturbance equations as the instability grows. The character of the initial conditions and boundary conditions in turn controls the path of non-linear break down of the laminar flow. However, the non-homogeneous boundary conditions are often unimportant because of the disparity in scales between the free-stream and boundary layer disturbances.

Since the unsteady free-stream disturbances generally have much larger wavelengths than those of the boundary layer eigenmodes, a mechanism to re-scale the free-stream disturbances is required for a strong coupling between the external and internal perturbations of the boundary layer. These mechanisms are found in rapid, localized

adjustments of the basic state. Thus, the classic receptivity sites are near surface roughness, and the model leading edge or stagnation point where a strong local pressure gradient exists and rapid boundary layer growth occurs. The stationary disturbances (i.e. Görtler and crossflow) apparently respond to streamwise vorticity generated at the leading edge or discrete roughness elements (Reibert and Saric 1997, Saric et al. 1998) so that this re-scaling is not necessarily required.

In a low-disturbance environment, the initial growth of the instability can be described by a set of linear disturbance equations (derived from the unsteady Navier-Stokes equations) valid in the limit of small disturbance amplitudes. As the amplitude increases, non-linear interactions occur that give rise to new secondary instabilities. The boundary layer becomes highly three-dimensional, instability growth is very rapid, and breakdown to turbulence occurs quickly. The final mechanism that leads directly to the chaotic and random fluctuations of turbulence is appropriately named the tertiary instability. However, the latter occurs over such a short distance, that there is usually no distinction made between the secondary and tertiary instabilities.

At times, the initial amplitude of the instability can be so strong that one or more stages of instability growth is "bypassed" (Morkovin 1984). Non-linear mechanisms lead to turbulence prematurely. The bypass mechanisms are poorly understood, but have been repeatedly observed in cases of high disturbance environment, including free-stream turbulence, sound (e.g. the conventional wind tunnel), sufficient roughness, and wall-waviness.

## 1.2.1 Boundary Layer Stability Prediction

### 1.2.1.1 Instability types

At the heart of the transition process is the presence of an instability within the boundary layer whose characteristics are governed by the basic state, free-stream conditions, disturbance environment, and surface geometry. The instability mechanisms that initiate the transition process (primary instability of Figure 1-3) are categorized by their physical mechanisms of instability growth as Tollmien-Schlichting (TS) and Mack-modes, Görtler vortices, crossflow vortices, and Rayleigh instabilities. Under enabling conditions, each instability can exist as a "natural" oscillation, whose growth is driven by a conversion of energy from the boundary layer basic state to the instability. Many applications will have more than one instability that co-exist, in which case, the more unstable disturbance will dominate over the others, and/or strong non-linear interactions between instabilities will occur.

The TS mode is a general description of a vorticity wave propagating through the layer in the streamwise direction (two-dimensional wave), or at an angle inclined to the streamwise direction (oblique wave). Mack (1969, 1984) has given a complete account of these waves for the compressible layer at supersonic and hypersonic speeds. In particular, he showed that (1) the oblique "first-mode" waves are more unstable than their two-dimensional counterpart, and (2) with increasing Mach number ( $M_e > 4$ ), a second-mode and additional "Mack-modes" with an acoustic nature become more unstable than the first-mode instability. The TS and Mack-modes are traditionally responsible for transition in flat plate and conical flows with a low-disturbance environment.



In the boundary layer on a concave wall (the general case is treated with streamline curvature rather than geometry curvature), the Görtler instability develops due to an imbalance between centrifugal forces and the pressure gradient normal to the wall. The outer regions of the boundary layer have a higher radial acceleration than the inner regions. Hence, the boundary layer exchanges fluid between the inner and outer regions with counter-rotating vortices whose axes are parallel to the streamwise coordinate.

A three-dimensional boundary layer provides the possibility for a crossflow instability associated with the inflection point in the lateral velocity profile. The inflection point is highly unstable and gives rise to spanwise modulations in the form of co-rotating vortex structures with their axes aligned with the inviscid streamlines. The vortex structure provides many similarities to the Görtler instability.

#### **1.2.1.2 Linearized theory**

The initial development of the primary instability can be described with linear stability theory (LST) in the limit of small amplitude disturbances. A harmonic perturbation is superimposed onto the undisturbed boundary layer state. If that perturbation grows, the layer is said to be unstable, and if all disturbances decay, the layer is stable. The LST has its roots in the unsteady Navier-Stokes equations linearized about the basic state. But the major simplifications in the theory come about by locally ignoring all boundary layer growth terms, and imposing homogeneous boundary conditions at the wall (smooth wall) and in the free-stream (no external disturbances). The resulting set of equations can be solved at any streamwise location with a given basic

state, and represents the correct zeroth-order approximation – formally justified with a complete nonparallel analysis.

Reed, Saric and Arnal (1996) have most recently reviewed linear stability theory. Mack (1969) still provides the most complete account of incompressible and compressible stability theory. Later he condensed this discussion and updated some of the issues in three-dimensional boundary layers and three-dimensional instabilities in (Mack 1984).

#### **1.2.1.3 Non-linear methods**

More sophisticated methods of stability prediction are the Parabolized Stability Equations (PSE) (Herbert 1997) and direct numerical solutions (DNS) of the Navier-Stokes equations (Reed 1993). The new PSE approach treats the boundary layer as a weakly non-parallel flow by including boundary layer growth terms, but neglecting streamwise diffusion in the disturbance equations. The result is a set of parabolic disturbance equations that are marched in the streamwise direction to analyze the evolution of single or interacting Fourier modes. Initial conditions are prescribed, presumably from experiment or a receptivity analysis. The DNS techniques remove all constraints of the stability problem, with an arbitrary spectrum of unsteady free-stream and surface conditions as input.

#### **1.2.2 Boundary Layer Transition Prediction**

Traditional engineering methods predict the onset of transition (defined by the first appearance of turbulent bursts) with empirical correlations. The simplest of these are

based on integral boundary layer parameters. Examples include the shape factor correlation of Wazzan (1981), or transition based on a momentum thickness Reynolds number  $Re_\theta$ . However, the physics of the instability growth, and receptivity are completely removed.

The most common method for transition prediction used in industry involves LST coupled with an  $e^N$  transition prediction scheme (Smith and Gamberoni 1956, Van Ingen 1956, Arnal 1993). Growth rates of the linear disturbance are calculated on the body with LST for a given frequency, wavelength, and disturbance orientation. Integrating the growth rates from the first unstable point to some downstream location gives the disturbance amplitude  $A$  relative to the initial disturbance amplitude  $A_o$ . Transition is said to occur when the initial disturbance  $A_o$  has been amplified to a certain threshold,  $e^N$ , where  $N$  is the so-called  $N$ -factor is defined by

$$N \equiv \ln \left( \frac{A_T}{A_o} \right) \quad (1-1)$$

The quantity  $A_T$  is the disturbance amplitude at transition. Since the  $e^N$  method can only correlate transition to the amplitude ratio, the role of receptivity in defining  $A_o$  is ignored entirely, and any effect of the disturbance environment must be included in the "calibrated" value of  $N$ . The primary utility in the  $e^N$  method is in comparing transition induced by the same primary instability between two similar disturbance environments. The  $N$ -factor can also be used as a stability index for parametric studies using the local amplitude  $A$  in place of  $A_T$ . At a given location, a lower value of  $N$  would indicate a more stable flow, and a longer run of laminar flow would be expected.

In low-disturbance environments, such as that found in quiet wind tunnels and free-flight, transition has been correlated to  $N \approx 9-11$  for a wide variety of two-dimensional bodies with TS instabilities in subsonic through hypersonic conditions (Malik 1989a, Arnal 1993). Computations by Malik (1989a) showed that transition on a flat plate and cone (recall Figure 1-2) at Mach 3.5 occur near  $N=10$ . Transition on the Dougherty and Fisher  $10^\circ$  sharp cone in flight also correlated  $9 < N < 11$ .

As a correlation, the method is equally applicable to compressible and incompressible boundary layers with steady Görtler, or crossflow instabilities. However, the vortex motion of these instabilities quickly causes non-linear distortion of the basic state; the use of LST all the way to the point of transition is highly questionable (Arnal 1993, Reed et al. 1996). For Görtler vortices, Floryan (1991) reports that about 50% of the total distance from the neutral point to transition onset is dominated by non-linear development, whereas TS instabilities have a linear development that covers 75% to 85% of the unstable region (Arnal 1993). Accordingly, the  $N$ -factor for stationary vortical disturbances implicitly includes a large extrapolation of the linear region to the location of transition onset, as well as the receptivity effects on  $A_o$ . It is not surprising that the  $e^N$  method shows a high-degree of scatter for Görtler and crossflow disturbances.

The PSE and DNS techniques allow transition prediction directly from the instability amplitude, since the value of  $A_o$  is required in the solution. The inclusion of non-linear effects also allows transition prediction methods more closely related to physical conditions in aircraft design like the point of minimum shear stress or minimum heat transfer – but at considerable computational expense.

### 1.2.3 Heat-Transfer Mechanisms in Stability and Transition

#### 1.2.3.1 Uniform heating

The hydrodynamic stability of a boundary layer is strongly controlled by the shape of the mean velocity profile in the boundary layer. It has been shown (Mack 1969) that the more negative the velocity second derivative is at the wall,  $(\partial^2 U/\partial y^2)|_{y=0}$ , the “fuller” and more stable the velocity profile becomes. This result applies to both inviscid and viscous instabilities. With an understanding of how  $(\partial^2 U/\partial y^2)|_{y=0}$  affects hydrodynamic stability, a class of stability modifiers (Gad-el-Hak 1990, see also section 3.7 of Reed et al. 1996) has been developed from the compressible stream-wise momentum equation applied at the wall,

$$\left[ \rho V \frac{\partial U}{\partial y} \right]_{y=0} + \frac{dP}{dx} - \frac{d\mu}{dT} \left[ \frac{\partial T}{\partial y} \frac{\partial U}{\partial y} \right]_{y=0} = \left[ \mu \frac{\partial^2 U}{\partial y^2} \right]_{y=0} \quad (1-2)$$

Note that differentiation has been performed on the viscous dissipation term to obtain the last term on the left hand side (LHS) and the term on the right in equation 1-2.

Among other modifiers (suction, controlled pressure gradient, etc.) the last term on the LHS is positive or negative depending on the direction of heat transfer. In air, the dynamic viscosity,  $\mu$ , always increases with temperature, therefore,  $d\mu/dT > 0$  and  $\partial U/\partial y|_{y=0} > 0$  for non-separating flows. If heat is removed from the fluid (wall cooling),  $\partial T/\partial y > 0$ , and the last term of the LHS is negative. The second derivative  $(\partial^2 U/\partial y^2)|_{y=0}$  becomes more negative showing a fuller and thus more stable velocity profile. Similarly, wall heating produces  $\partial T/\partial y < 0$ , bringing the second derivative closer to zero, and

destabilizing the boundary layer. This heating effect has been verified in a number of experiments on cones and flat plates. In fact, Lees (1946), and later Reshotko (1963) showed the possibility that at low supersonic Mach numbers, a boundary layer can be completely stabilized with cooling below some threshold ratio of cooled wall to adiabatic wall temperature.

However, the arguments related to equation 1-2 (the "classical heat transfer effect") apply to the boundary layer stability governed by first-mode TS waves. Other modes of instability, such as the Mack modes (Mack 1984), Görtler vortices (Floryan 1991), and crossflow instabilities (Reed et al. 1996) do not respond to the heat transfer effect in the same way as discussed above, and may show an opposite heat transfer effect.

Analysis of Görtler vortices for incompressible and compressible flows shows a mixed response to surface heating. At supersonic speeds, El-Hady and Verma (1983, 1984) used a normal mode solution to show that the stabilizing or destabilizing effects is dependent upon the choice of parameters in the problem. Spall and Malik (1989) solved the full Görtler problem with a marching procedure (linear PSE) to improve the solution of El-Hady and Verma, explore the effect of pressure gradient, and extend the results to wall heating at supersonic and hypersonic Mach numbers. At Mach 3.5, Spall and Malik show that heating has a mild stabilizing effect (doubling the wall temperature gave a 15% increase in  $Re_T$  at  $N=10$ ) and cooling is slightly destabilizing – an apparent monotonic trend. Growth rates with and without heating at other Mach numbers were not presented.

The stability trends with surface heating or cooling for the compressible Görtler problem are rationalized against the relative dominance of viscous dissipation

(stabilizing) and centrifugal forces (destabilizing) (El-Hady and Verma 1984, Kabayashi and Kohoma 1977).

### 1.2.3.2 Localized Heating

Recently, the possibilities of stabilizing first-mode TS waves in a boundary layer by localized heating have been explored in subsonic flows. There are relatively few papers on the subject (most in Russian), but the reported effects are all consistent.

Masad and Nayfeh (1992) demonstrated, theoretically, that the boundary layer over a flat plate could be notably stabilized when the heating strips are properly placed ahead of the neutral stability point. Heating the boundary layer upstream causes the boundary layer to be "cooled" upon entering the region of instability. Therefore, by the classical cooling effect of equation 1-2, the velocity profile instead becomes more stable, thus moving transition onset downstream. Placing the heat transfer strips inside the unstable region (i.e. downstream of the neutral point), increased the growth rates at and downstream of the strip – again showing the relevance of equation 1-2. Masad and Nayfeh calculated the opposite behavior when cooling strips were used in place of the heating strips. Both incompressible and compressible flows (up to  $M=0.8$ ) were included in the study.

The same "natural cooling" effect has also been confirmed in several flat-plate experiments (Dovgal et al. 1990, Maestrello and Nagabushana 1989). Dovgal et al. showed by experiment that when heat was concentrated at and near the leading edge, the growth of unstable waves was reduced. If heat was placed in the unstable region, the boundary layer became more unstable. With proper location of the heating, transition

Reynolds number could be increased by as much as 70% over the adiabatic case, with only a 28% increase in the local wall temperature. Transition could even be delayed with heating at the leading edge in even the presence of a three-dimensional square roughness element.

Kazakov et al. (1995) have also applied the localized heating technique to the leading edge of a two-dimensional airfoil to show substantial increases in the transition Reynolds number in the chord-wise direction. When intense heating was used, transition delay could even be demonstrated with a thermally insulated surface downstream of the initial heating. These results were in qualitative agreement with the experiments of McCroskey (1961, quoted in Maestrello 1990) whose results were again attributed to natural cooling.

Maestrello (1990) also reports the local surface heating as a means for relaminarizing a turbulent boundary layer proceeding a concave surface with Görtler vortices. With an initially turbulent boundary layer heat is applied in the appropriate location, and the relaminarization produces the famous Blasius profile. Relaminarization is again attributed to natural cooling downstream of the heater, according to the stability arguments of equation 1-2.

### **1.3 State of the Art in Quiet Wind Tunnels**

As described in Section 1.1, the natural state of the boundary layer on the nozzle walls is the most common cause of a noisy environment which in turn causes poor results from transition experiments conducted in wind tunnels. Figure 1-5 shows a schematic of how transition on the nozzle walls defines the low-disturbance test core of the quiet



tunnel. The forward region of the test rhombus is defined by the Mach lines that extend forward from the nozzle exit, while the back of the test core is limited by the Mach lines that emanate from an acoustic source at the wall – e.g. the onset of boundary layer transition. If the distance between the apex of the opposing wedges (or cones in an axisymmetric tunnel) is  $\Delta x$ , then the Reynolds number at the free-stream conditions in the test rhombus, based on  $\Delta x$  ( $Re_{\Delta x}$ ) represents the largest Reynolds number that can be tested within the quiet test core. The primary objective in quiet tunnel design is to maximize  $Re_{\Delta x}$  by maintaining laminar flow on the nozzle walls as long as possible. The largest “quiet-flow Reynolds number” achieved in practice to date has been  $Re_{\Delta x} = 9 \times 10^6$  in the Langley Mach 3.5 pilot tunnel (Chen and Malik 1990).

Before discussing the LFC techniques employed to maximize  $Re_{\Delta x}$ , we must address the question: What constitutes quiet flow? The database of atmospheric disturbances in the flight environment is sparse, and cannot be used for a quantitative comparison to the wind tunnel environment. In the absence of these direct measurements, the best working definition of “quiet-flow” would be derived from a comparison of  $Re_T$  in the wind tunnel and flight. Beckwith et al. (1983) have used the Dougherty and Fisher 10° cone data and corresponding low-disturbance wind tunnel tests (Figure 1-2) to suggest a level of static pressure fluctuations less than 0.05% of the mean for quiet flow. Another common threshold is pitot pressure (i.e. total pressure behind a normal shock wave) fluctuations that are less than 0.1% of the mean (Beckwith et al. 1983, Wolf et al. 1994, Wolf and Laub 1996). In either case, the disturbance spectra should also be monotonic decreasing with increasing frequency (Reshotko 1997b).

### 1.3.1 Boundary Layer Development on a Supersonic Nozzle

To achieve "quiet" operation, a solid understanding is needed of transition in the boundary layers growing on the interior surfaces of the wind tunnel nozzle and test section. A necessary element in this understanding is the behavior of the nozzle laminar boundary layer, on the basis of which stability calculations and accompanying transition predictions can be made.

Most nozzle designs are either of the two-dimensional type or axisymmetric, each with its inherent advantages. The two-dimensional nozzle consists of two opposing contoured nozzle blocks enclosed within two flat sidewalls. Flow sections are rectangular, with expansion taking place in a direction parallel to the sidewalls. At any given distance from the nozzle throat, the inviscid flow is therefore laterally uniform on the contoured surfaces, but is strongly variable on the sidewalls. Specifically, pressure gradients appear on the sidewalls in a direction normal to the main flow vector, inducing crossflows which distort the sidewall boundary layers and generate appreciable three-dimensionalities in the corners (King and Demetriades 1993, Ostrander et al. 1989). The resultant laminar boundary layer profiles around the periphery of any given cross-section are thus non-uniform, also leading to potential non-uniformities in the boundary layer stability and transition to turbulence. The laminar boundary layer development of the two-dimensional nozzles has been most recently addressed with experimental and theoretical analyses by Demetriades et al. (1998). Axisymmetric tunnels enjoy some simplicity in the boundary layer development, since the inviscid flow and boundary layer development at any given distance from the throat are independent of the angular coordinate. Boundary layer stability and transition are also

expected to be nominally axisymmetric. However, the fabrication and visual access of axisymmetric tunnels are more difficult to achieve than with a two-dimensional shape.

### 1.3.2 Nozzle Design Features for Laminar Flow Control and Noise Reduction

To summarize the history of quiet nozzle development (Beckwith and Miller 1990), the primary causes of nozzle wall turbulence have been found to be roughness in the nozzle throat, continuation of the turbulent boundary layer in the settling chamber and contraction into the nozzle, and destabilization of the nozzle wall laminar boundary layer by the formation and amplification of instabilities which subsequently grow and cause a turbulent wall boundary layer. These issues are addressed by providing a highly polished nozzle, suction slot upstream of the throat to remove the turbulent boundary layer (i.e. "bleed slots"), and a slow-expansion axisymmetric nozzle to reduce the strength of Görtler vortices, and increase the axial distance of the quiet test core based on Mach lines from the "acoustic origin" of the turbulent boundary layer.

It would appear that the techniques for maintaining natural laminar flow by optimizing the nozzle geometry have been exhausted. Yet, the present achievable transition Reynolds numbers on nozzle walls (and hence quiet test core size) still impose severe limitations for studying natural transition at flight conditions in the wind tunnel. It therefore remains to explore other LFC methods to further increase  $Re_{\Delta x}$ . One such method appears to be a controlled temperature distribution on the nozzle surface.

### 1.3.3 Observed Temperature Effects on Nozzle Boundary Layers

In 1975, Harvey et al. investigated the effect of heating the surface in a Mach 5 pilot supersonic nozzle as part of a quiet wind tunnel design. Strip heaters were placed around the outside of the nozzle surface and subsonic approach. The results showed the transition Reynolds number increased by approximately 20%. The heating in these experiments, however, was not applied locally, as in the work of Masad and Nayfeh (1992), but uniformly over the nozzle surface. The probable mechanism of transition delay was explained as a result of an increased boundary layer thickness with heating that, in turn, reduced the relative height of surface roughness (Harvey et al. 1975a). Thus, the surface heating produced a "smoother" surface. The finding that heat could delay transition was apparently overshadowed by the two-fold increase in  $Re_T$  produced by boundary layer bleed-slots, and was not pursued further.

Through the 1978-1981 period, Demetriades (1978, 1981a, 1981b, 1992a) studied the effect of surface roughness and wall temperature on the boundary layer in the throat of the MSU Mach 3 supersonic wind tunnel. Liquid nitrogen was circulated through ducts in the nozzle throat region located approximately 1 cm below the exposed surface of the aluminum nozzle block. Transition Reynolds numbers were seen to monotonically decrease with decreasing wall temperature (Figure 1-4). This result was again in opposition to the simpler theory for flat plate flows.

In 1993, Demetriades (1996) returned to the nozzle heating effect to confirm the observations of Harvey et al. (1975) and Demetriades (1981a, 1992a) and explain why heating or cooling delays or promotes transition, respectively. A uniform heat flux was

applied with a film heater that began upstream of the throat, and extended to 70% of the nozzle length. With surface temperatures only about 12% above the adiabatic wall temperature, the boundary layer state could be reduced from turbulent to laminar (Demetriades 1996). It was hypothesized that the heat concentrated near the nozzle throat caused a natural cooling of the boundary layer downstream, and thus a more stable boundary layer by the classical cooling effect.

Very recently, similar trends have been observed with a cold wall promoting transition in the Purdue Mach 4 Ludwig Tube (Munro 1996, Schneider 1997).

#### **1.4 Purpose of This Investigation**

If the apparent heating effect can be optimized (e.g. heating level, location) and transferred to other wind tunnel facilities, implications on quiet wind tunnel technology can be far reaching. Moreover, if instability growth, and thus transition, can be substantially delayed by local heating in a wind tunnel, the acoustic origin of noise produced by the transitional and turbulent boundary layer will be moved down-stream, and the quiet test core will be enlarged for a given set of stagnation conditions.

The review of the current literature clearly shows that the heating effect on the nozzle boundary layer has remained largely unexplained from either an experimental or theoretical viewpoint. And furthermore, direct measurements of boundary layer transition, even without surface heating, on the interior surfaces of a wind tunnel nozzle are scarce. The objectives of the present investigation have been to explore physical mechanisms responsible for the observed delay in transition on the wind tunnel nozzle when heat is applied.

- (1) Linear stability theory was applied to the boundary layer of a quiet supersonic nozzle to identify linear stability mechanisms associated with and without surface heating on the wind tunnel nozzle.
- (2) The unsteady oscillations preceding the onset of boundary layer transition on a wind tunnel nozzle were measured both with and without surface heating.
- (3) The results of the experiment and those of linear stability theory were compared.

With a favorable comparison between the theory and experiment, surface heating techniques could be applied to new and existing low-disturbance facilities with confidence using a rational design approach. However, if the theory could not predict the experimental observations with acceptable accuracy, the measurements themselves could provide more insight into the physics of the surface heating and guide the way for further study.

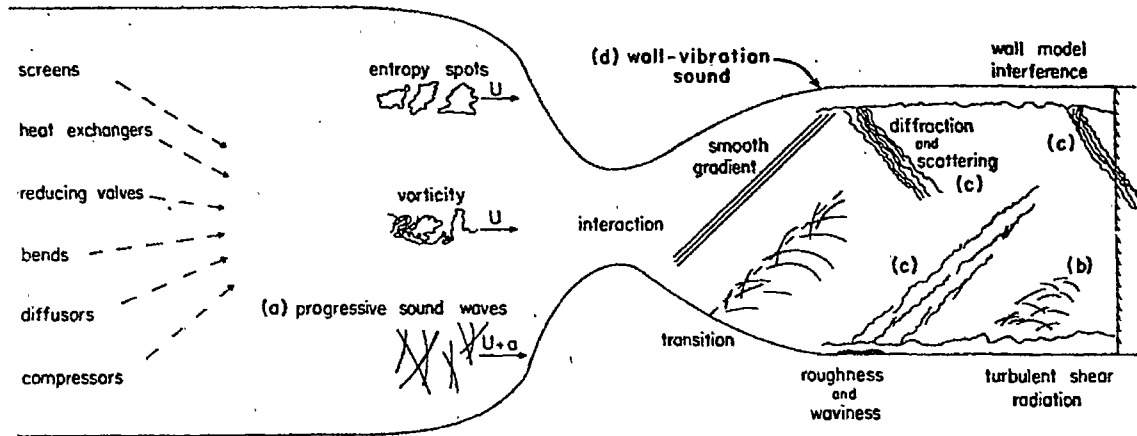


**Figure 1-1. Unsteady disturbances found in a supersonic wind tunnel. Acoustic radiation from group (c) is the most common cause of premature transition in a supersonic wind tunnel model. Adapted from (Morkovin 1959).**

































































































































































































































































































































































































































































